Volume 1 | Number 1 | Jan 2013 | Pages 1–100

Chemical Science

www.rsc.org/chemicalscience

ROYAL SOCIETY OF CHEMISTRY

This is an *Accepted Manuscript*, which has been through the Royal Society of Chemistry peer review process and has been accepted for publication.

Accepted Manuscripts are published online shortly after acceptance, before technical editing, formatting and proof reading. Using this free service, authors can make their results available to the community, in citable form, before we publish the edited article. We will replace this *Accepted Manuscript* with the edited and formatted *Advance Article* as soon as it is available.

You can find more information about *Accepted Manuscripts* in the **Information for Authors**.

Please note that technical editing may introduce minor changes to the text and/or graphics, which may alter content. The journal's standard **Terms & Conditions** and the **Ethical guidelines** still apply. In no event shall the Royal Society of Chemistry be held responsible for any errors or omissions in this *Accepted Manuscript* or any consequences arising from the use of any information it contains.

www.rsc.org/chemicalscience

Chemical Science

EDGE ARTICLE

Au^I Cl-bound N-heterocyclic carbene ligands form M^II_4(LAuCl)_6 integrally gilded cages

William J. Ramsay, Jonathan A. Foster, Katharine L. Moore, Tanya K. Ronson, Raphaël J. Mirgalet, David A. Jefferson and Jonathan R. Nitschke[*]

The incorporation of an N-heterocyclic carbene (NHC) moiety into a self-assembled $M^{II}_4L_6$ cage framework required the NHC first to be metallated with gold(I). Bimetallic cages could then be constructed using zinc(II) and cadmium(II) templates, showing weak luminescence. The cages were destroyed by the addition of further gold(I) in the form of $Au^I(2,4,6$-trimethoxybenzonitrile)$_2$SbF$_6$, which caused the reversibly-formed cages to disassemble and controllably release the Au^I-NHC subcomponent into solution. This release in turn induced the growth of gold nanoparticles. The rate of dianiline release could be tuned by capsule design or through the addition of chemical stimuli, with different release profiles giving rise to different nanoparticle morphologies.

Introduction

A variety of multitopic ligands have been designed to self-assemble with metal ions in order to construct three-dimensional metal-organic structures.[1] Many of the novel applications of these supramolecular assemblies derive from the chemical functionalities of their incorporated ligands.[2-13] As new rules are established to allow ligands incorporating more reactive groups to be built into supramolecular assemblies, new types of functionality can arise.[14]

The shape and dimensions of discrete, self-assembled supramolecular structures are predominantly dictated by how ligands with a characteristic size and denticity come together in geometries defined by the coordination sphere of a given metal ion.[15-28] The functionality[29-36] of these assemblies can be shaped by incorporating ligands with active functional groups, which can also be modified *in situ* either pre-[37-40] or post-synthetically.[41-44] The response of a ligand to an external stimulus, such as light, can influence the guest binding affinity of the corresponding supramolecular structure.[45] When a ligand contains a coordinated transition metal that is catalytically active, this active site can be orientated explicitly by the supramolecular framework, either protecting or exposing it;[46] incorporating more than one metal center thus can allow for division of labor between structural and functional metal centers.

Department of Chemistry, University of Cambridge, Lensfield Road, Cambridge CB2 1EW, UK. E-mail: jrn34@cam.ac.uk

N-heterocyclic carbenes (NHCs) are a useful class of electron-donating ligands that form strong metal-ligand bonds.[47] Gold(I)-NHCs, in particular, have found applications in the fields of catalysis,[48] pharmaceuticals,[49] liquid crystals[50] and optical devices.[51, 52] Despite the potential of incorporating metal-based NHC ligands into supramolecular constructs, opening new possibilities of control over their reactivity, few examples of self-assembled structures with this motif have been reported.[53-56] We thus designed subcomponent **A** and its metallated carbene derivatives **B − D** (Scheme 1), to be capable of reversibly self-assembling with 2-formylpyridine and metal ions to form supramolecular structures, in order to probe the scope and limitations of the ability of this class of ligand to self-assemble into supramolecular structures. As Au^I-NHC complexes can be reduced to form carbene-stabilized gold nanoparticles (Au NPs),[57] we anticipated that incorporating this ligand motif into a reversibly formed supramolecular structure could allow for new means to be developed to control the nucleation and growth conditions of Au NPs.

Results and discussion

Subcomponent syntheses and cage preparation

The syntheses of NHC dianilines **A − D** were accomplished as shown in Scheme 1. Imidazolium **A** was prepared through reduction of a *bis*-azido imidazolium precursor (Scheme S1), prepared as described in the Supporting Information. Taking advantage of the established ability of NHCs to coordinate to many metal ions,[55] metallocarbenes **B − D** were prepared by metallating **A** following established, straightforward procedures.[53, 58, 59]

These subcomponents were subjected to conditions that were anticipated to lead to the preparation of self-assembled

$M^{II}_4L_6$ structures.[25] Each was treated in turn with 2-formylpyridine and the prospective metal templates Zn^{II}, Cd^{II}, Fe^{II} and Co^{II}. Although dianilines **A** – **C** did not yield discrete complexes with any of these templates, and **D** with Fe^{II} or Co^{II} gave intractable mixtures of products, **D** (6 equiv) was observed to generate metal-organic cages **1** and **2** following treatment with 2-formylpyridine (12 equiv) and either zinc(II) or cadmium(II) di[bis(trifluoromethylsulfonyl)imide] (triflimide, NTf_2^-; 4 equiv) respectively, as the uniquely observed products in solution (Figure 1; Supporting Information Sections 1.3 and 1.4). Confirmation of the $M^{II}_4L_6$ stoichiometry was provided by electrospray ionization mass spectrometry (ESI MS; Figures S10a and S20b), including high resolution MS (Figures S10b and S20b).
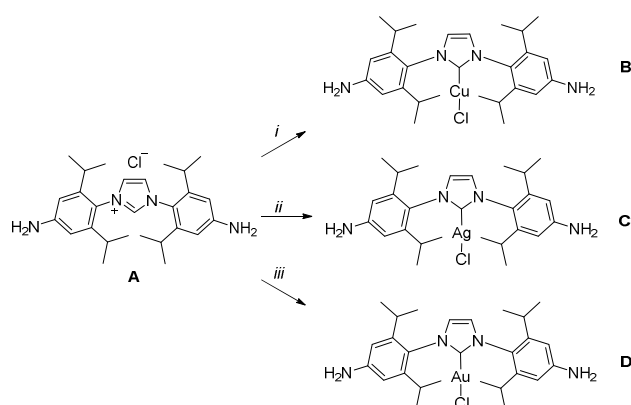

Scheme 1 Syntheses of subcomponents **A** – **D**. *Reaction conditions:* (i) CuCl, Na_2CO_3, acetone, 60 °C, 16 h, 90%; (ii) Ag_2O, DCM, 25 °C, 2 h, 90%; (iii) Au(tht)Cl, aq. Na_2CO_3, DCM, 25 °C, 0.5 h, 92%.

The observation that dianilines **A** – **C** did not lead to discrete cage formation suggested that a strong and inert metal-NHC bond was required in the ligand to construct a cage, which was provided by the gold(I) chloride moiety in **D**. Fluorescence spectroscopy for both **1** and **2** in dry acetonitrile (Figures S11 – S12 and S21 – S22, respectively) indicated weak luminescence, with bands that are attributed to both intra- and intermolecular $Au^{I}\cdots Au^{I}$ interactions, as observed in gold(I)-containing supramolecular architectures developed by Yam and co-workers.[60] The removal of the gold-bound chloride from ligand **D** in cages **1** and **2** following the addition of chloride-binding metal cations, such as stoichiometric Ag^{I} or excess Zn^{II} or Cd^{II} (Figures S13 – S14 and Figures S23 – S24) caused disassembly, suggesting that Coulombic repulsion between adjacent ligands destabilized the cage framework. Agents that engender the removal of chloride, therefore, provided a stimulus to trigger the response of cage destruction.

NMR spectra for the products **1** and **2** (Figures S5 and S15, respectively) yielded three imine signals. In the case of **2**, satellite signals associated with the imines were observed, attributed to *J*-coupling with the two spin-1/2 isotopes of cadmium.[61] The three magnetically inequivalent ligand

environments observed in both the ^1H and ^{13}C NMR spectra of the cages suggested that the achiral S_4 (ΛΛΔΔ) diastereomer of a M_4L_6 framework was present in solution, but not the homochiral *T* (ΔΔΔΔ/ΛΛΛΛ) or heterochiral C_3 (ΔΔΔΛ/ΛΛΛΔ) diastereomers.[62, 63] The steric bulk of the isopropyl groups is expected to hold the phenyl rings orthogonal to the central imidazolium ring; this coplanar orientation of the terminal phenylene rings has been shown to favor a *syn* arrangement of the ligands,[64] making the S_4-symmetric framework the lowest-energy conformation, and thus the unique product observed in solution. Diffusion ordered spectroscopy (DOSY) was consistent in each case with all signals belonging to a single species (Figures S9 and S19). The ^{19}F NMR signal for NTf_2^- was unchanged from its free value in cages **1** and **2**, consistent with the absence of anion encapsulation (Figures S6 and S16).
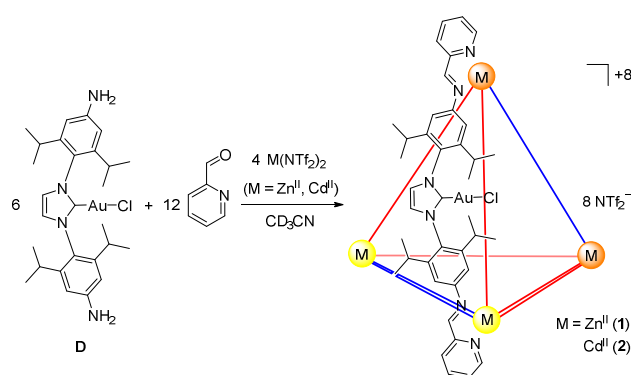
Fig. 1 Dianiline **D** was the only dianiline observed to form $Zn^{II}_4L_6$ (**1**) and $Cd^{II}_4L_6$ (**2**) cages through subcomponent self-assembly. These cages are inferred to have approximate S_4 symmetry, consisting of two Δ (orange) and two Λ (yellow) metal vertices and two *anti* (blue) and four *syn* ligands (red). Only one (*syn*) ligand is shown for clarity.

In order to visualize the cage geometry, an energy-minimized model of **2** in the S_4 arrangement[65] was constructed (Figure 2b) based upon the X-ray crystal structure of **D** (Figure 2a). The achiral framework is composed of two metal centers of the same handedness (Λ) and two metal centers of opposite handedness (Δ). Each pair of metal centers of the same stereochemistry is connected by ligands adopting *anti* conformations (where the –AuCl moieties are directed to the outside of the cage), and the other four ligands are *syn* (where the –AuCl moieties are directed inwards); we acknowledge that other conformations may be possible in solution. Our model suggests that the cages are sufficiently flexible to allow the gold(I) centers to approach each other, accounting for the weak luminescence associated with the presence of gold-gold interactions (further modelling of the intermolecular cage interactions in **2** is provided in Figure S22).

a

b
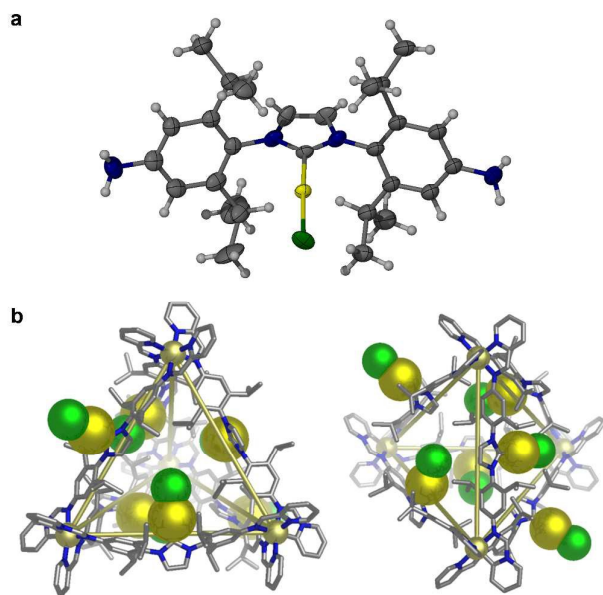
Fig. 2 (a) ORTEP representation of the crystal structure of **D**, showing thermal ellipsoids at 40% probability level. Solvent molecules and disorder are omitted for clarity. (b) Two views of a model of the MM2[66] energy-minimized structure of **2**. The –AuCl units are shown in space-filling representation. Hydrogens and counterions are omitted for clarity (color scheme: carbon, grey; nitrogen, blue; cadmium, light yellow; gold, dark yellow; chloride, green).

Nanoparticle synthesis

Amines have been shown to reduce cationic gold species to Au^0 and to cap the gold nanoparticles (Au NPs) formed following growth.[67-70] Dianiline **D** thus possesses two useful characteristics in this context: it can reduce a gold source to Au^0 (which can be stabilized by the oxidized aniline) and the NHC coordinated Au^I can also participate in the formation of Au NPs, stabilized by the available carbene. The reduction of a soluble Au^I source in acetonitrile (Au(tmbn)$_2$SbF$_6$; tmbn = 2,4,6-trimethoxybenzonitrile) for Au NP growth was thus investigated in two cases: with dianiline **D** alone, and when **D** was incorporated into cages **1** and **2**.

Following the addition of Au(tmbn)$_2$SbF$_6$ (6 equiv) to a solution of **1** in dry acetonitrile (Supporting Information Section 3.1), the surface plasmon resonance (SPR) band in the UV-Vis spectrum, attributable to Au NPs,[71] was observed to grow in following a sigmoidal time course with steps corresponding to nucleation, growth, and saturation (Figure 3a); consistent growth features were observed in a second run (Figure S26). When cadmium-containing cage **2** was mixed with Au(tmbn)$_2$SbF$_6$ (6 equiv) (Supporting Information Section 3.2), the SPR band in the UV-Vis spectra began to grow in intensity approximately 22 min after mixing (Figure 3a), a delay 10 min longer than was observed in the case of **1** (Figure S36). In both experiments, NP growth was observed only after part of the cage had first disassembled (Figures S27 – S28 and S37 – S39). When cage **1** decomposed to provide the reducing agent, TEM (Figure S29) and AFM (Figure S30) images displayed aggregates (250 nm in diameter) of approximately

5 nm Au NPs, together with Au NPs approximately 50 nm in diameter (Figure 3b), following 90 min of NP growth. In contrast, when cage **2** disassembled {111}-faceted triangular prisms approximately 300 nm in edge length were observed (Figure 3b), in addition to aggregates of 5 nm Au NPs (Figures S40 and S41). Particle size distribution analysis of AFM measurements confirmed the presence of the larger triangular species alongside numerous small NP (Figure S41d-h); the triangular features constituted approximately 10% of the species counted, but approximately 52% of the total gold.
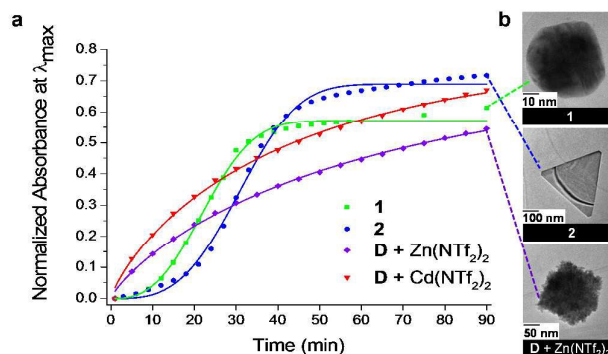
Fig. 3 (a) The evolution of the SPR UV-Vis band was monitored during Au NP formation when the reducing agent employed was provided by cages **1** and **2** and with **D** and either Zn(NTf$_2$)$_2$ or Cd(NTf$_2$)$_2$; the curves were fitted using the Avrami equation[72, 73] (Supporting Information Section 3.6). (b) Differences in Au NP morphology observed in the TEM images for growth conditions shown in (a).

We also observed that when reagent grade acetonitrile (0.01% H$_2$O) was used in place of the anhydrous solvent (<0.001% H$_2$O) during the synthesis of Au NPs with cage **2**,[74] the SPR band in the UV-Vis spectra appeared more rapidly (Figure S42). We infer that the higher water content of the solvent increased the rate of imine hydrolysis in **2**, resulting in a shortening of the nucleation stage. Instead of the triangular prisms observed with anhydrous solvent, TEM images revealed hexagonal plates (Figure S42) and aggregates of 5 nm particles. This difference in Au NP morphology may be attributed to the variation in the rate of cage breakdown.

Notably, control experiments involving equimolar quantities of **D**, Zn(NTf$_2$)$_2$ or Cd(NTf$_2$)$_2$ and Au(tmbn)$_2$SbF$_6$ (Supporting Information Sections 3.1.1 and 3.2.1) resulted in a SPR band in the UV-Vis spectra immediately following mixing (Figure 3a) and significantly different NP morphologies. When equimolar quantities of **D** and Zn(NTf$_2$)$_2$ were mixed with Au(tmbn)$_2$SbF$_6$, only aggregates were observed in the TEM images (Figure 3b); nanoparticles greater than 5 nm in diameter were not observed in contrast to the case when **1** provided reductant **D** through its hydrolysis. In addition, none of the anisotropic Au NP morphologies grown starting from **2** were observed in the control experiment involving equimolar quantities of **D**, Cd(NTf$_2$)$_2$ and Au(tmbn)$_2$SbF$_6$. Further control experiments in which only **A** or **D** were used in the reduction of Au^I (Supporting Information Sections 3.3 and 3.4, respectively) revealed similarly rapid rates of formation and small nanoparticle morphologies in the presence of either Cd^{II}

or Zn[II]. Energy-dispersive X-ray spectroscopy (EDS) confirmed the presence of gold (with small quantities of nitrogen) across all experiments (Figures S29, S32, S40 and S44), with a higher organic content observed in the aggregates of smaller Au NPs compared to the larger anisotropic species; spectral features consistent with Zn or Cd were not observed, suggesting that these metals were not incorporated into the NPs. The aggregation of the Au NPs and the observation of organic material in the EDS spectra suggested that the oxidized bis-monodentate ligand **D** may have acted to bridge between Au NPs, as has been observed with similar ligands.[75]

The kinetics of Au NP formation were assessed with the Avrami theoretical model for crystallization and growth[72, 73, 76] (Supporting Information Section 3.6). In the Avrami equation, the overall kinetics are described by the apparent rate parameter k_{app} which depends principally upon the nucleation rate – a slower k_{app} is attributed to a lengthier nucleation stage.[77] The k_{app} of Au NP growth when **1** provided the reducing agent was 1.8×10^{-4} (the units are min^{-n} for all rate constants), with an Avrami exponent (n) of 2.59; in a control experiment using **D** and Zn(NTf$_2$)$_2$ as reductant, the rate constant was 1.70×10^{-2} with an exponent of 0.97. Similarly, Au NP growth where the reducing agent was provided by **2** provided displayed a rate constant of 1.5×10^{-6} with an exponent of 3.4, and the control experiment using **D** and Cd(NTf$_2$)$_2$ gave a k_{app} of 3.8×10^{-2} with an exponent of 0.90 (Table S1). As the Avrami exponent n[78-82] has been inferred to reflect the nucleation mechanism and directionality of growth, the constant nucleation rate ($n \approx 1$) observed when **D** served as the reductant with different metal salts is consistent with the observation of spherical Au NPs. Similarly, the multi-dimensional growth ($n > 1$) observed when **1** or **2** were used as reductants is consistent with a heterogeneous nucleation mechanism being responsible for the anisotropic features.[72] The rate constants and Avrami exponents observed when **1** and **2** were used as reductants suggest that the supramolecular structures impeded Au^0 nucleation, in contrast to the faster nucleation observed when free **D** was present in solution.

Mechanistically, we infer that the addition of Au^I to a solution of **1** or **2** first resulted in the abstraction of chloride, as noted above in the cases of other metal salts. This destabilizes the cage and results in its disassembly and release of free subcomponent **D**. We attribute the difference in rate of dianiline release between **1** and **2** to the differences in thermodynamic stabilities between these two structures. The shorter nucleation stage provided by the breakdown of **1** in comparison to the longer nucleation stage provided by **2** is consistent with the labile Zn[II] centers that have a faster kinetics of ligand exchange;[83] it is this delay during the nucleation stage of Au NP growth that ultimately determines the final NP size and shape. The slow rate of **D** release from **1** and **2** thus brought about a longer nucleation stage and slower rate of Au^I reduction, as required to produce thermodynamically-favored shapes with low-index facets, such as the {111}-faceted triangular prisms.[84] Several other factors, including the presence of small amounts of different salts

(such as ZnCl$_2$ or CdCl$_2$ from cage decomposition, or the metal triflate salts) could also influence the final particle shape and kinetics of nanoparticle growth,[84] but the control experiments involving **D** and Zn[II] or Cd[II] were not consistent with this mechanism. The different growth rates and morphologies of the observed Au NPs were thus inferred to result from the incorporation of an Au^I-NHC dianiline ligand into the walls of metal-organic capsule as the diimine.

Conclusions

We have reported the synthesis of NHC-containing dianilines **A** – **D**, and demonstrated that subcomponent **D** alone was able to form supramolecular cages with zinc(II) and cadmium(II), thanks to the protection afforded to the reactive carbene center by the Au^{I}Cl moiety; we anticipate that similarly inert metal-bound NHC complexes, such as Pt(II)-NHC,[85] could also be used to this effect. The removal of this gilding resulted in cage decomposition, which could be productively used in order to build up Au NPs of controllably variable morphologies. This supramolecular approach to modulating the rate of release of reducing agent affords a means of indirectly programming the morphology of Au NPs through reversible protection of the reducing amines within dynamic imine linkages. Our method circumvents the need to directly control the rate of reductant release, as is currently required in order to control Au NP morphology.[84] The reagent release profile is governed by the thermodynamic stability of the supramolecular structure and can be purposely altered by adding chemical stimuli that disrupts cage stability. Although this method of control is prohibitively expensive, the controllable nonlinearity of response that we observed may be of interest in the context of signal transduction in complex chemical networks.[86]

Acknowledgements

Notes and references

1   T. R. Cook and P. J. Stang, *Chem. Rev.*, 2015, **115**, 7001-7045.
2   J. M. Rivera, T. Martín and J. Rebek, *Science*, 1998, **279**, 1021-1023.
3   T. Liu, Y. Liu, W. Xuan and Y. Cui, *Angew. Chem. Int. Ed.*, 2010, **49**, 4121-4124.
4   P. D. Frischmann, S. H. M. Mehr, B. O. Patrick, F. Lelj and M. J. MacLachlan, *Inorg. Chem.*, 2012, **51**, 3443-3453.
5   S. Mirtschin, A. Slabon-Turski, R. Scopelliti, A. H. Velders and K. Severin, *J. Am. Chem. Soc.*, 2010, **132**, 14004-14005.
6   M. M. J. Smulders, S. Zarra and J. R. Nitschke, *J. Am. Chem. Soc.*, 2013, **135**, 7039-7046.
7   J. S. Mugridge, G. Szigethy, R. G. Bergman and K. N. Raymond, *J. Am. Chem. Soc.*, 2010, **132**, 16256-16264.

8   R. Custelcean, P. V. Bonnesen, N. C. Duncan, X. Zhang, L. A. Watson, G. Van Berkel, W. B. Parson and B. P. Hay, *J. Am. Chem. Soc.*, 2012, **134**, 8525-8534.

9   S. K. Samanta and M. Schmittel, *Org. Biomol. Chem.*, 2013, **11**, 3108-3115.

10   R. Frantz, C. S. Grange, N. K. Al-Rasbi, M. D. Ward and J. Lacour, *Chem. Commun.*, 2007, 1459-1461.

11   S. Mecozzi and J. J. Rebek, *Chem. Eur. J.*, 1998, **4**, 1016-1022.

12   G. Zhang, O. Presly, F. White, I. M. Oppel and M. Mastalerz, *Angew. Chem. Int. Ed.*, 2014, **53**, 5126-5130.

13   M. Han, J. Hey, W. Kawamura, D. Stalke, M. Shionoya and G. H. Clever, *Inorg. Chem.*, 2012, **51**, 9574-9576.

14   K. Liu, Y. Kang, Z. Wang and X. Zhang, *Adv. Mater.*, 2013, **25**, 5530-5548.

15   B. Olenyuk, J. A. Whiteford, A. Fechtenkotter and P. J. Stang, *Nature*, 1999, **398**, 796-799.

16   B. F. Abrahams, S. J. Egan and R. Robson, *J. Am. Chem. Soc.*, 1999, **121**, 3535-3536.

17   M. Eddaoudi, J. Kim, J. B. Wachter, H. K. Chae, M. O'Keeffe and O. M. Yaghi, *J. Am. Chem. Soc.*, 2001, **123**, 4368-4369.

18   H. Arora, J. Cano, F. Lloret and R. Mukherjee, *Dalt. Trans.*, 2011, **40**, 10055-10062.

19   R. W. Saalfrank, A. Stark, K. Peters and H. G. von Schnering, *Angew. Chem., Int. Ed. Engl.*, 1988, **27**, 851-853.

20   N. Takeda, K. Umemoto, K. Yamaguchi and M. Fujita, *Nature*, 1999, **398**, 794-796.

21   P. Mal, B. Breiner, K. Rissanen and J. R. Nitschke, *Science*, 2009, **324**, 1697-1699.

22   H. T. Chifotides, I. D. Giles and K. R. Dunbar, *J. Am. Chem. Soc.*, 2013, **135**, 3039-3055.

23   M.-K. Chung, K. Severin, S. J. Lee, M. L. Waters and M. R. Gagne, *Chem. Sci.*, 2011, **2**, 744-747.

24   T. Weilandt, U. Kiehne, J. Bunzen, G. Schnakenburg and A. Lützen, *Chem. Eur. J.*, 2010, **16**, 2418-2426.

25   T. K. Ronson, S. Zarra, S. P. Black and J. R. Nitschke, *Chem. Commun.*, 2013, **49**, 2476-2490.

26   J. Dömer, J. C. Slootweg, F. Hupka, K. Lammertsma and F. E. Hahn, *Angew. Chem.*, 2010, **122**, 6575-6578.

27   X.-P. Zhou, Y. Wu and D. Li, *J. Am. Chem. Soc.*, 2013, **135**, 16062-16065.

28   S. Pasquale, S. Sattin, E. C. Escudero-Adán, M. Martínez-Belmonte and J. de Mendoza, *Nat. Commun.*, 2012, **3**, 785.

29   L. Isaacs, *Acc. Chem. Res.*, 2014, **47**, 2052-2062.

30   P. Ballester, *Chem. Soc. Rev.*, 2010, **39**, 3810-3830.

31   H.-J. Schneider and A. K. Yatsimirsky, *Chem. Soc. Rev.*, 2008, **37**, 263-277.

32   M. I. Sánchez, J. Mosquera, M. E. Vázquez and J. L. Mascareñas, *Angew. Chem. Int. Ed.*, 2014, **53**, 9917-9921.

33   S. J. Edwards, H. Valkenier, N. Busschaert, P. A. Gale and A. P. Davis, *Angew. Chem. Int. Ed.*, 2015, **54**, 4592-4596.

34   K. Yazaki, Y. Sei, M. Akita and M. Yoshizawa, *Nat. Commun.*, 2014, **5**.

35   J. Kang, J. Santamaría, G. Hilmersson and J. Rebek, *J. Am. Chem. Soc.*, 1998, **120**, 7389-7390.

36   D. J. Cram, M. E. Tanner and R. Thomas, *Angew. Chem., Int. Ed. Engl.*, 1991, **30**, 1024-1027.

37   L. M. Hancock, L. C. Gilday, S. Carvalho, P. J. Costa, V. Félix, C. J. Serpell, N. L. Kilah and P. D. Beer, *Chem. Eur. J.*, 2010, **16**, 13082-13094.

38   G. Barin, M. Frasconi, S. M. Dyar, J. Iehl, O. Buyukcakir, A. A. Sarjeant, R. Carmieli, A. Coskun, M. R. Wasielewski and J. F. Stoddart, *J. Am. Chem. Soc.*, 2013, **135**, 2466-2469.

39   I. Pochorovski, M.-O. Ebert, J.-P. Gisselbrecht, C. Boudon, W. B. Schweizer and F. Diederich, *J. Am. Chem. Soc.*, 2012, **134**, 14702-14705.

40   Y. Li and A. H. Flood, *Angew. Chem. Int. Ed.*, 2008, **47**, 2649-2652.

41   K. K. Tanabe and S. M. Cohen, *Chem. Soc. Rev.*, 2011, **40**, 498-519.

42   P. L. Golas and K. Matyjaszewski, *Chem. Soc. Rev.*, 2010, **39**, 1338-1354.

43   D. Konkolewicz, A. Gray-Weale and S. Perrier, *J. Am. Chem. Soc.*, 2009, **131**, 18075-18077.

44   D. A. Roberts, A. M. Castilla, T. K. Ronson and J. R. Nitschke, *J. Am. Chem. Soc.*, 2014, **136**, 8201-8204.

45   M. Han, R. Michel, B. He, Y.-S. Chen, D. Stalke, M. John and G. H. Clever, *Angew. Chem. Int. Ed.*, 2013, **52**, 1319-1323.

46   H. J. Yoon, J. Kuwabara, J.-H. Kim and C. A. Mirkin, *Science*, 2010, **330**, 66-69.

47   M. N. Hopkinson, C. Richter, M. Schedler and F. Glorius, *Nature*, 2014, **510**, 485-496.

48   D. Gatineau, J.-P. Goddard, V. Mouriès-Mansuy and L. Fensterbank, *Isr. J. Chem.*, 2013, **53**, 892-900.

49   E. R. T. Tiekink, *Crit. Rev. Oncol. Hematol.*, 2002, **42**, 225-248.

50   P. Espinet, *Gold Bull.*, 1999, **32**, 127-134.

51   R. Visbal, I. Ospino, J. M. López-de-Luzuriaga, A. Laguna and M. C. Gimeno, *J. Am. Chem. Soc.*, 2013, **135**, 4712-4715.

52   D. M. Roundhill and J. P. Fackler, *Optoelectronic Properties of Inorganic Compounds*, Springer USA, 2013.

53   C. E. Willans, K. M. Anderson, P. C. Junk, L. J. Barbour and J. W. Steed, *Chem. Commun.*, 2007, 3634-3636.

54   T. Fahlbusch, M. Frank, G. Maas and J. Schatz, *Organometallics*, 2009, **28**, 6183-6193.

55   I. J. B. Lin and C. S. Vasam, *Can. J. Chem.*, 2005, **83**, 812-825.

56   C. Mejuto, G. Guisado-Barrios, D. Gusev and E. Peris, *Chem. Commun.*, 2015, DOI: 10.1039/C1035CC05114B.

57   J. Vignolle and T. D. Tilley, *Chem. Commun.*, 2009, 7230-7232.

58   A. Hospital, C. Gibard, C. Gaulier, L. Nauton, V. Thery, M. El-Ghozzi, D. Avignant, F. Cisnetti and A. Gautier, *Dalton Trans.*, 2012, **41**, 6803-6812.

59   O. Santoro, A. Collado, A. M. Z. Slawin, S. P. Nolan and C. S. J. Cazin, *Chem. Commun.*, 2013, **49**, 10483-10485.

60   X.-F. Jiang, F. K.-W. Hau, Q.-F. Sun, S.-Y. Yu and V. W.-W. Yam, *J. Am. Chem. Soc.*, 2014, **136**, 10921-10929.

61   W. Meng, T. K. Ronson and J. R. Nitschke, *Proc. Natl. Acad. Sci. USA*, 2013, **110**, 10531-10535.

62   A. M. Castilla, W. J. Ramsay and J. R. Nitschke, *Acc. Chem. Res.*, 2014, **47**, 2063-2073.

63   D. L. Caulder, C. Brückner, R. E. Powers, S. König, T. N. Parac, J. A. Leary and K. N. Raymond, *J. Am. Chem. Soc.*, 2001, **123**, 8923-8938.

64   W. Meng, J. K. Clegg, J. D. Thoburn and J. R. Nitschke, *J. Am. Chem. Soc.*, 2011, **133**, 13652-13660.

65   T. Beissel, R. E. Powers, T. N. Parac and K. N. Raymond, *J. Am. Chem. Soc.*, 1999, **121**, 4200-4206.

66   CAChe Workspace, WorkSystem Pro Version 7.5.0.85.

67   M. Aslam, L. Fu, M. Su, K. Vijayamohanan and V. P. Dravid, *J. Mater. Chem.*, 2004, **14**, 1795-1797.

68   S. Gomez, K. Philippot, V. Colliere, B. Chaudret, F. Senocq and P. Lecante, *Chem. Commun.*, 2000, 1945-1946.

69   X. Lu, M. S. Yavuz, H.-Y. Tuan, B. A. Korgel and Y. Xia, *J. Am. Chem. Soc.*, 2008, **130**, 8900-8901.

70 C. Subramaniam, R. Tom and T. Pradeep, *J. Nanopart. Res.*, 2005, **7**, 209-217.
71 W. Haiss, N. T. K. Thanh, J. Aveyard and D. G. Fernig, *Anal. Chem.*, 2007, **79**, 4215-4221.
72 Y. Zhou, W. Lin, F. Yang, W. Fang, J. Huang and Q. Li, *Chem. Phys.*, 2014, **441**, 23-29.
73 M. Avrami, *J. Chem. Phys*, 1940, **8**, 212-224.
74 HPLC grade acetonitrile was purchased from Fisher Scientific with a 0.008% water content (max. 0.01%). Anhydrous acetonitrile (99.8%) was purchased from Sigma Aldrich with a < 0.001% water content.
75 M. Orbach, M. Lahav, P. Milko, S. G. Wolf and M. E. van der Boom, *Angew. Chem. Int. Ed.*, 2012, **51**, 7142-7145.
76 P. N. Njoki, J. Luo, M. M. Kamundi, S. Lim and C.-J. Zhong, *Langmuir*, 2010, **26**, 13622-13629.
77 M. L. Di Lorenzo and C. Silvestre, *Prog. Polym. Sci.*, 1999, **24**, 917-950.
78 A. T. W. Kempen, F. Sommer and E. J. Mittemeijer, *J. Mater. Sci.*, 2002, **37**, 1321-1332.
79 T. A. Baker, O. L. A. Monti and D. J. Nesbitt, *J. Phys. Chem. C*, 2011, **115**, 9861-9870.
80 S. Ranganathan and M. Von Heimendahl, *J. Mater. Sci.*, 1981, **16**, 2401-2404.
81 J. P. Gaviría, L. G. Navarro and A. E. Bohé, *J. Phys. Chem. A*, 2012, **116**, 2062-2070.
82 G. Oyama, Y. Yamada, R.-i. Natsui, S.-i. Nishimura and A. Yamada, *J. Phys. Chem. C*, 2012, **116**, 7306-7311.
83 I. A. Riddell, Y. R. Hristova, J. K. Clegg, C. S. Wood, B. Breiner and J. R. Nitschke, *J. Am. Chem. Soc.*, 2013, **135**, 2723-2733.
84 M. L. Personick and C. A. Mirkin, *J. Am. Chem. Soc.*, 2013, **135**, 18238-18247.
85 E. A. Baquero, J. C. Flores, J. Perles, P. Gómez-Sal and E. de Jesús, *Organometallics*, 2014, **33**, 5470-5482.
86 D. Ray, J. T. Foy, R. P. Hughes and I. Aprahamian, *Nat. Chem.*, 2012, **4**, 757-762.

Chemical Science Accepted Manuscript